International Immunopharmacology 66 (2019) 1–12

Contents lists available at ScienceDirect

International Immunopharmacology

journal homepage: www.elsevier.com/locate/intimp

Pinellia pedatisecta lectin exerts a proinflammatory activity correlated with ROS-MAPKs/NF-κB pathways and the NLRP3 inflammasome in RAW264.7 cells accompanied by cell pyroptosis

Wei Wang[a,1], Shanhu Mao[a,1], Hongli Yu[a,b,c,d,*], Hao Wu[a,b,c,d,*], Xuelian Shan[a], Xingde Zhang[a,e], Guojing Cui[e], Xianqiong Liu[f]

[a] School of Pharmacy, Nanjing University of Chinese Medicine, Nanjing 210023, China
[b] Jiangsu Key Laboratory of Chinese Medicine Processing, Nanjing University of Chinese Medicine, Nanjing 210023, China
[c] Engineering Center of State Ministry of Education for Standardization of Chinese Medicine Processing, Nanjing 210023, China
[d] State Key Laboratory Cultivation Base for TCM Quality and Efficacy, Nanjing University of Chinese Medicine, Nanjing 210023, China
[e] Yancheng Traditional Chinese Medicine Hospital Affiliated to Nanjing University of Chinese Medicine, Yancheng 224000, China
[f] Pharmacy Faculty, Hubei University of Chinese Medicine, Wuhan 430065, China

ARTICLE INFO

Keywords:
Pinellia pedatisecta
Lectin
ROS
MAPK and NF-κB/NLRP3 pathways
IL-1β
Pyroptosis

ABSTRACT

Pinellia pedatisecta, a widely used herb in Chinese medicine, has proinflammatory toxicity related to its *Pinellia pedatisecta* lectin (PPL), but the mechanism is still unknown. However, for safer use, it is necessary to clarify its proinflammatory mechanism. Herein, we studied the mechanism in RAW264.7 cells. PPL decreased the mitochondrial membrane potential (MMP) and increased the outflow of calcium, accompanied by the overproduction of reactive oxygen species (ROS), which resulted in the activation of the MAPK and NF-κB pathways and the release of IL-1β. The maturation of IL-1β relied on caspase-1 p20, the active caspase-1, as demonstrated by adding caspase-1 inhibitor. While caspase-1 was associated with the activation of the NLRP3 inflammasome, we further found that the stimulation of PPL also contributed to the activation. In addition, TXNIP was downregulated, whereas NLRP3/caspase-1 p20/ASC was upregulated, and there was binding of TXNIP with NLRP3. There was also binding of NLRP3 with ASC and caspase-1. Further, we found that *N*-acetylcysteine (NAC), an ROS scavenger, could inhibit the PPL-stimulated activation of these pathways and the release of IL-1β. Moreover, PPL led to cell pyroptosis with pyknotic nuclei and plasma membrane rupture, which could be inhibited by NAC. All of these findings demonstrated an important role of ROS in the inflammation caused by PPL. Taken together, our data provide new mechanistic insights into the possible endogenous signaling pathways involved in the inflammation of RAW264.7 cells, stimulated by PPL.

1. Introduction

Pinellia pedatisecta Schott, a widely used Chinese medicine for relieving cough and reducing sputum, belongs to the Araceae family [1]. Our previous research had proved that *P. pedatisecta* demonstrated toxicity due to the *Pinellia pedatisecta* lectin (PPL), which has been proven to be the main component causing inflammation [2,3]. We have previously verified that PPL could cause mouse peritoneal macrophages to release large amounts of ROS and IL-1β [4]. ROS are known as second messengers in mediating inflammation responses [5]. In the process of inflammation, the production of ROS increases, thereby activating the MAPK and NF-κB signaling pathways [6,7], which results in an abnormal MMP and the release of calcium ions and cytokines [8–11]. Since the MAPK and NF-κB signaling pathways can be activated by certain irritants including excess ROS [12,13], they can increase the level of pro-IL-1β. This, in turn, is activated to become IL-1β, which can exert biological activity [14–16]. Whether the inflammation caused by PPL was related to the MAPKs or to the NF-κB signaling pathway is still under consideration.

Studies have also revealed that ROS may be the key factor regulating the NLRP3 inflammasome [17–19], a multiprotein complex consisted of NLRP3, apoptosis-associated speck-like protein containing a CARD (ASC), and Caspase-1, but the specific relationship between ROS and NLRP3 remains unclear. As far as what can be determined,

* Corresponding authors at: School of Pharmacy, Nanjing University of Chinese Medicine, Nanjing 210023, China.
E-mail addresses: yuhongli76@163.com (H. Yu), whao5795@163.com (H. Wu).
[1] These authors contributed equally to this work.

https://doi.org/10.1016/j.intimp.2018.11.002
Received 26 July 2018; Received in revised form 1 November 2018; Accepted 1 November 2018
Available online 08 November 2018
1567-5769/

thioredoxin (TRX) and thioredoxin-interacting protein (TXNIP) are currently known to be involved in NLRP3 activation [20,21]. After the NLRP3 inflammasome is formed, the caspase-1 may be activated to caspase-1 p20, which can promote pro-IL-1β to become IL-1β [22]. Therefore, we studied whether the proinflammatory response caused by PPL was associated with the activation of the NLRP3 inflammasome. We also studied how PPL acts on the proteins of the inflammasome and on the protein–protein interactions inside the inflammasome. Since caspase-1 p20 can promote pro-IL-1β to become IL-1β, we further researched if that suggested a close relationship between the ROS, MAPK, and NF-κB pathways and the NLRP3 inflammasome during the inflammation caused by PPL.

In our previous study, inflammation caused by PPL was related to the overproduction of ROS and IL-1β [4]. Nevertheless, the signaling pathways that lead to the activation of IL-1β induced by PPL are still little known. In this study, using cultured RAW264.7 cells, we explored whether PPL initiated a chain reaction, including the activation of the MAPK and NF-κB pathways and the NLRP3 inflammasome, the activation of caspase-1, and the production of IL-1β. In addition, we unraveled the mechanism for the proinflammatory activity of PPL. We hope this work provides new perspectives for the development of the detoxification processing of *P. pedatisecta*.

2. Materials and methods

2.1. Medicinal materials

P. pedatisecta was collected from Jiangsu Province (China) in May 2016 and then authenticated in Jiangsu Institute for Food and Drug Control by Professor Haobin Hu.

2.2. Reagents and antibodies

Phenyl Sepharose™ high performance and Q Sepharose™ high performance were purchased from GE Healthcare (10249526, 10226682; Uppsala, Sweden). FBS (Fetal Bovine Serum) was bought from Beyotime Institute of Biotechnology (C0232; Beijing, China). DMEM (Dulbecco's modified eagle's medium) was obtained from HyClone (SH30022.01; Logan, UT, USA). ROS assay kit was provided by Nanjing Jiancheng Bioengineering Institute (E004; Nanjing, China). Anti-NLRP3, anti-TRX, anti-p38/p-p38, anti-JNK/p-JNK, anti-ERK/p-ERK and prestained Pageruler™ protein ladder were purchased from Abcam (ab214185, ab26320, ab170099, ab47363, ab112501, ab4821, ab17942, ab201015; Cambridge Science Park, UK). Anti-caspase-1 p20 was from Santa Cruz Biotechnology (sc-398715; 2145 Delaware Ave, USA). Anti-IκB-α and anti-NF-κB-p65 antibodies were bought from Easybio (BE3385-50, BE3154-100; Beijing, China). Anti-phospho-IκBα antibody, anti-pro-IL-1β were provided by Cell Signaling (4814,12507S; Boston, USA). Anti-ASC and anti-TXNIP antibodies were obtained from Cell Signaling (67824S, 14715S; Boston, MA, USA). RIPA lysis buffer, PMSF, anti-GAPDH antibody, Goat anti-rabbit lgG (H + L) HRP and Mouse IL-1β ELISA kit were supplied by Yifeixue Biotech Co., Ltd. (YWB001, YP0100-10, YT0065-500, YT1010, YT0020-100, YFPA1059, YFSA02, YFXEM00028; Nanjing, China). LPS (Lipopolysaccharides) from *Escherichia coli* 055:B5 was purchased from SIGMA (L2880; Merck KGaA, Darmstadt, Germany). Immobilon®-P transfer membrane, Immobilon Western chemiluminescent HRP substrate and immunoprecipitation Kit-Dynabeads™ protein G were bought from Thermo Fisher Scientific (IPVH00010, WBKLS0500, 10007D; Massachusetts, USA). Enhanced BCA protein assay kit, Cy3-labeled donkey anti-goat IgG (H + L), FITC-labeled goat anti-rabbit IgG (H + L), DAPI dihydrochloride, immunostaining permeabilization solution with Triton X-100, 5 × SDS-PAGE sample loading buffer, MMP kit with JC-1, and cytoplasmic and nuclear protein extraction kits were bought from Beyotime Institute of Biotechnology (P0010, A0502, A0562, C0016, P0016, P0015, AF0234, P0028; Shanghai, China). DynaMag™-Spin was supplied by Life Technologies (2514; Massachusetts, USA). Glass bottom cell culture dish was obtained from NEST (061217Q01; Wuxi, China).

2.3. Extraction, separation and identification of PPL

Tubers of *Pinellia pedatisecta* (700 g) were peeled, chopped and homogenized. Centrifugation (10,000 *g*, 30 min) was conducted to obtain the supernatant. Its volume was calculated, and saturated ammonium sulfate ($(NH_4)_2SO_4$) solution was slowly added under magnetic stirring to a saturation of 45%. The solution was centrifuged again (10,000 *g*, 15 min) to obtain the precipitate that was then completely dissolved in 0.6 mol/L saturated $(NH_4)_2SO_4$ solution. The main peak was collected after hydrophobic analysis (velocity: 2 mL/min; sample size: 5–10 mL; eluent: 0.6 mol/L–0 mol/L sulfate solution in 60 min). Then the main peak was collected after ion exchange chromatography (eluent: 0 mol/L–1 mol/L sodium chloride solution in 60 min; flow rate: 2 mL/min). After dialysis and freeze-drying, purified PPL was obtained.

2.4. SDS-PAGE and SEC-HPLC (size-exclusion high performance liquid chromatograph)

To determine subunit molecular weight, SDS-PAGE was performed for the purified PPL with a 15% (*w/v*) acrylamide gel. The PPL sample was denatured with SDS-PAGE sample loading buffer and boiled for 10 min. Subsequently, the acrylamide gel was stained by silver nitrate. The molecular weight of sample protein was matched with that of standard marker. Meanwhile, PPL was also detected with an Agilent 1200 system equipped by a diode array detector, and a 9.4 × 250 mm Agilent Zorbax GF-450 column was employed. PBS (0.1 mol/L) at the flow rate of 1.5 mL/min was used as the mobile phase.

2.5. In-gel digestion, LC-MS/MS and database search

The band at 13 kDa was decolored by 30% acetonitrile (400 μL) in 100 mM NH_4HCO_3 solution, reduced by 100 mM dithiothreitol (10 μL) for 30 min at 56 °C, dehydrated by acetonitrile (100 μL), alkylated by 200 mM iodoacetamide (30 μL) for 20 min in dark at room temperature, dehydrated again by acetonitrile (100 μL) and finally dried. In-gel digestion was conducted using trypsin for 20 h at 37 °C. The resulting peptides were extracted three times, each time by 60% acetonitrile (100 μL) for 15 min in 0.1% formic acid. The obtained peptides were dried, reconstituted by 0.1% formic acid and 5% acetonitrile in water, and then analyzed with an LTQ VELOS LC-LTQ system (Thermo Finnigan, San Jose, CA, USA). They were collected by a Zorbax 300SB-C18 peptide reverse-phase trap column (Agilent Technologies, Wilmington, DE, USA) and thereafter eluted into a 0.15 × 150 mm RP-C18 analytical column (Column Technologies Inc., Lombard, IL, USA). The mobile phase consisted of A (84% acetonitrile with 0.1% formic acid) and B (0.1% solution of formic acid at pH 3.0), and the flow rate was 0.15 mL/min. First, 4% solvent A was used and held for 4 min, which was elevated to 50% solvent A linearly within 15 min and to 100% within 3 min. Peptides were detected by an ESI mass spectrometer in the positive-ion mode. The spray voltage and temperature were 3.2 kV and 200 °C respectively. The collision energy was automatically set with the LTQ system. Full MS scan and ten MS/MS scans for the most intense ions were performed. Protein was identified by MS/MS raw data based on the UniProt Arecaceae protein database and the BioWorks Browser 3.3 searching program (University of Washington, Seattle, WA, USA; licensed to Thermo Finnigan), according to the criteria of Xcorr (three charges ≥3.75, two charges ≥2.2, one charge ≥1.9) and Delta CN (≥0.1).

2.6. Cell culture

RAW264.7 cells were bought from the Type Culture Collection of

the Chinese Academy of Sciences (Shanghai, China), cultured in DMEM (100 U/mL penicillin G potassium, 10% FBS and 100 μg/mL streptomycin) and incubated in a 37 °C incubator with 5% CO_2.

2.7. Detection of ROS, MMP, and cytosolic free Ca^{2+} concentrations

Intracellular ROS levels were detected by DCFH-DA, an oxidation-sensitive fluorescent probe. After penetrating cells, DCFH-DA is hydrolyzed into non-fluorescent DCFH by intracellular esterase, and the latter can be quickly oxidized into highly fluorescent DCF when ROS are present. RAW264.7 macrophages were cultured in 48-well culture plates. These cells were divided into 6 groups: Group 1 was given PBS, as a blank control group. Group 2 was given 5 μg/mL LPS, as a positive control group. Groups 3–6 were given PPL at 6.25, 12.5, 25, and 50 μg/mL, respectively. DCFH-DA (4 μM) was added to the cell culture dish for 20 min at 37 °C after treatment with PPL for 1 h. The fluorescence intensities were detected by a fluorescence microplate reader (PerkinElmer, Waltham, MA, USA), with excitation and emission wavelengths of 488 and 525 nm, respectively.

MMP was measured with fluorescence microscopy by using JC-1 as the probe. RAW264.7 macrophages were cultured in DMEM in 48-well culture plates. These cells were divided into 6 groups: Group 1 was given PBS, as a blank control group. Group 2 was given carbonyl cyanide 3-chlorophenylhydrazone, as a positive control group. Groups 3–6 were given PPL at 6.25, 12.5, 25, and 50 μg/mL, respectively, for 1 h. Then 5 μL of JC-1 staining solution (Beyotime Institute of Biotechnology, Shanghai, China) was added into each well. Subsequently, the samples were incubated in darkness for 20 min at 37 °C in a 5% CO_2 incubator. The cells were thereafter washed three times with buffer solution and analyzed with a Leica fluorescence microscope (Wetzlar, Germany). The red:green fluorescence ratio was detected by the fluorescence microplate reader.

To measurement the cytosolic free Ca^{2+} concentrations, cells were cultivated in black 96-well plates. The grouping of cells was the same as for the detection of ROS. Then the cells were loaded with Fluo-4 following the kit's instructions. Following 30 min of incubation, the fluorescence microplate reader was used (excitation: 494 nm; emission: 516 nm). The experiments above were all repeated six times.

2.8. Western blot testing of MAPK and NF-κB/NLRP3 pathways and pro-IL-1β

RAW264.7 cells were cultured in 100 mm × 20 mm style dishes (Corning, #430167). The grouping of cells was the same as for the detection of ROS. After stimulation with PPL for 1 h with or without pretreatment with NAC, the cells were homogenized in RIPA lysis buffer. The supernatants were frozen and stored at −80 °C. Cell homogenates were denatured with SDS-PAGE sample loading buffer and boiled for 10 min. Samples were applied to a 10% (w/v) acrylamide gel according to the BCA assay, transferred onto polyvinylidene difluoride membranes at 100 V for about 1 h, and blocked in 5% BSA for 2 h. The membranes were probed with appropriate antibody or anti-GAPDH overnight at 4 °C, incubated with secondary antibody for 2 h, and then visualized with a FujiFilm LAS-4000 mini Luminoimage analyzer (Tokyo, Japan). GAPDH served as a loading control. The experiments above were all repeated three times.

2.9. Measurement of IL-1β

For IL-1β induction, RAW264.7 macrophages were cultured in 48-well culture plates. The grouping of cells was the same as for the detection of ROS. Plates were incubated for 1 h, and all supernatants were collected. The level of IL-1β released from the macrophages was detected with corresponding ELISA kits following the kit instructions.

The formation and release of the inflammatory factor IL-1β is mediated by its precursor protein pro-IL-1β under caspase-1 p20 [22,23]. To clarify the role of caspase-1 p20 during the release of IL-1β under the stimulation of PPL, different doses of AC-TYR-VAL-ALA-ASP-CMK (Ac-YVAD-cmk) (0.1, 0.5, 2.5, and 12.5 μmol/L), an inhibitor of caspase-1, were applied. After pretreatment with this caspase-1 inhibitor for about 0.5 h, PPL (50 μg/mL) was added to the cells. They were then incubated for 1 h, and all supernatants were collected. The level of IL-1β released from the macrophages was detected with corresponding ELISA kits following the kit instructions. The experiments above were all repeated six times.

2.10. Co-immunoprecipitation assay

RAW264.7 cells were cultured in 100 mm × 20 mm style dishes. The grouping of cells was the same as for the detection of ROS. After stimulation for 1 h, the cells were homogenized in RIPA lysis buffer. Proteins were immunoprecipitated from extracts with anti-TXNIP (ab188865, Abcam), anti-TRX (ab26320, Abcam) or anti-NLRP3 (ab4207, Abcam). Dynabeads were resuspended completely by rotating on a roller for 5 min, and then 50 μL of the Dynabeads were transferred to a tube. The tube was then placed on a magnet and the supernatant was removed. Then the Dynabeads were resuspended in 200 μL of Ab binding and washing buffer which also contained the Ab of choice. The tube was incubated for 10 min with rotation at room temperature and the supernatant was removed. The Dynabead-Ab complex formed by resuspension was washed in 200 μL of Ab binding and washing buffer (without any antibody). Afterwards, the tube was placed on the magnet to remove the supernatant. Each antigen-containing sample was added to the Dynabead–Ab complex and gently resuspended by pipetting. Then the supernatant was transferred into a clean tube. The complex was washed three times using 200 μL of washing buffer for each wash and mixed gently by pipetting. Subsequently, the complex was resuspended in 100 μL of washing buffer, and the suspension was transferred into a clean tube. Then the Dynabead–Ab–antigen complex was gently resuspended in 20 μL of elution buffer, 10 μL of 5 × SDS-PAGE sample loading buffer was added, and the sample was incubated for 10 min at 70 °C. The tube was thereafter placed on the magnet and the sample was loaded onto a gel. Finally, the total proteins were extracted. Western blot methods were the same as above. The experiments were repeated three times.

2.11. Immunofluorescence staining

The colocalization of NLRP3 with caspase-1/ASC was examined by immunofluorescence staining. Cells were cultured in a confocal culture dish. The cells were divided into 6 groups: group 1, 1 mL/dish PBS only (control); groups 2–5, 1 mL/dish PPL (6.25, 12.5, 25, or 50 μg/mL). The LPS group had LPS added to a final concentration of 5 μg/mL. After stimulation for 1 h, the cells were fixed with 4% paraformaldehyde and permeabilized with 0.2% Triton X-100 for 10 min at room temperature. Then BSA was added dropwise for blocking at room temperature for 1 h. The cells were incubated for 2 h at 4 °C with goat anti-NLRP3 (1:200; Abcam, ab4207), rabbit anti-ASC (1:800; CST, 67824) and rabbit anti-caspase-1 (1:200; Abcam, ab1872) antibodies. Dishes were placed in wet boxes and incubated overnight at 4 °C. On the second day, double immunofluorescent staining was performed with FITC or cy3-labeled secondary antibody (1:500, Beyotime) for 1 h in darkness. DAPI was added to the culture dish to stain the nucleus. In each procedure, the cells were washed three times with PBS for 10 min each time. The dishes were visualized through sequential scanning on a Nikon laser scanning confocal microscope (Ti-E-A1R, Nikon, Japan). Colocalization was analyzed by Image J software. The experiments were repeated six times.

2.12. Analysis of the mode of death of RAW264.7 cells under PPL treatment

In order to analyze the mode of death of RAW264.7 cells stimulated with PPL, Hoechst 33342 and propidium iodide (PI) probes were used. That is, RAW264.7 cells were treated for 1 h with PPL (6.25, 12.5, 25, and 50 μg/mL) or PPL (50 μg/mL) for 0, 0.5, 1, 2, 3, or 4 h, respectively. To clarify the relationship between ROS and pyroptosis, different doses of NAC (0.1, 0.5, 2.5, or 12.5 mmol/L) were applied for 30 min. RAW264.7 cells were then washed with PBS and Hoechst 33342, and PI probes were added to each sample in accordance with the kit instructions. After incubation for about 30 min at 4 °C, the RAW264.7 cells were examined with a Leica fluorescence microscope (Wetzlar, Germany). The experiments were repeated six times.

2.13. Statistical analysis

Statistical analysis was conducted by SPSS v. 23.0 for Windows (SPSS, Chicago, IL, USA) using the Mann-Whitney *U* test. Numerical data were expressed as mean ± SD. $P < 0.05$ was considered statistically significant.

3. Results

3.1. Extraction, separation and identification of PPL

The main chromatogram peak was obtained by elution with gradient concentrations of NaCl solutions, and then detected by SEC-HPLC which presents a single HPLC peak (Fig. 1B). Tryptophan (0.2 kDa), insulin (5.7 kDa), ovalbumin (44 kDa), and bovine serum albumin (66.4 kDa) were used as standard markers (Fig. 1A). According to the standard curve (Fig. 1C), the native molecular weight of the extract PPL was approximately 13 kDa, which was consistent with a single band at 13 kDa (Fig. 1D) after SDS-PAGE. The molecular weight of PPL was consistent with previous research results [24,25]. PPL was then subjected to proteomic analysis by gel electrophoresis in combination with LC-MS/MS. The band at 13 kDa then underwent in-gel digestion by trypsin. Peptides were extracted from this band, loaded into an LC-MS/MS, and identified. Based on a protein database, the band at 13 kDa was identified as PPL. Fig. 1E–H present MS/MS for certain peptides from PPL.

3.2. Measurement of ROS, MMP, and outflow of cytosolic free Ca^{2+}

In our study, PPL caused the production of larger quantities of ROS in a dose-dependent manner compared with the quantity produced by the PBS group (Fig. 2A, B). LPS (5 μg/mL) was used as a positive control, which could increase the production of ROS. Further, we found that MMP was decreased (Fig. 2C, D). Indeed, 50 μg/mL PPL led to nearly a two-fold decrease in MMP. Carbonyl cyanide 3-chlorophenylhydrazone (cccp) (10 μmol/L) was used as a positive control, which could decrease the MMP. The amount of free Ca^{2+} (cytosolic) was increased fifteen-fold (Fig. 2E) with 50 μg/mL PPL, and LPS (5 μg/mL) was used as a positive control, which could increase the amount of free Ca^{2+}.

3.3. Immunoblot analysis of MAPK and NF-κB signaling pathways

Three major participants are included in the MAPK pathway: p38, ERK, and JNK [26]. These are involved in the regulation of cell proinflammatory states, proliferation, differentiation, and cell-cell function synchronization, and also play crucial roles in various cell events such as inflammatory responses [27]. The NF-κB signal transduction pathway (particularly p65 together with its inhibitory protein IκB) also plays a crucial role in inflammatory responses [28,29]. In our study, the phosphorylation of p38, JNK, ERK, p65, and IκB was enhanced after stimulation with different concentrations of PPL (Fig. 3A, B). LPS (5 μg/mL) was used as a positive control, which could increase the expressions of the phosphorylation of p38, JNK, ERK, p65, and IκB. We found that 50 μg/mL PPL led to nearly a five-fold increase in all of these proteins' phosphorylation levels, which indicated that PPL was related to the activation of the MAPK and NF-κB pathways.

3.4. Measurement of IL-1β and pro-IL-1β together with the NLRP3 signaling pathway-related proteins from RAW 264.7 macrophages

IL-1β is an important inflammatory cytokine that is converted to a mature form by its precursor protein pro-IL-1β, under the mediation of caspase-1, and then secreted into the extracellular region to exert its biological function [16]. In our study, PPL caused the release of large quantities of IL-1β (Fig. 3C). We found that 50 μg/mL PPL led to a three-fold increase in IL-1β together with a three-fold increase of pro-IL-1β compared to PBS treatment (Fig. 3D). LPS (5 μg/mL) was used as a positive control, which could increase the productions of IL-1β and pro-IL-1β. When an inhibitor of caspase-1 (AC-YVAD-CMK) was applied, the level of IL-1β decreased (Fig. 3E), which demonstrated an important role of caspase-1 during the inflammation caused by PPL.

Mature IL-1β is produced through cleavage of inactive pro-IL-1β by caspase-1, which is activated by the NLRP3 inflammasome [30]. In order to study the involvement of the NLRP3 inflammasome in inflammation caused by PPL, western blot was used to detect NLRP3 inflammatory signaling pathway-related proteins after treatment with PPL. When the NLRP3 inflammasome is activated, the levels of caspase-1 p20, NLRP3, and ASC increase [14]. Consistently, the levels of caspase-1 p20, NLRP3, and ASC were dose-dependently upregulated after stimulation with different concentrations of PPL (6.25, 12.5, 25, and 50 μg/mL, 1 h) (Fig. 3F). Additionally, TXNIP was downregulated by PPL. LPS (5 μg/mL) was used as a positive control. Therefore, the NLRP3 inflammasome plays an important role in PPL-induced inflammation.

3.5. Co-immunoprecipitation assay for the separation of TXNIP and TRX, and the combination of TXNIP and NLRP3

TRX is a scavenger of intracellular oxides. When cells are resting, TRX binds TXNIP [31]. In contrast, TRX self-oxidizes when cells generate large amounts of ROS, ROS could separate TRX and TXNIP complexes, and then TXNIP activate NLRP3 [32]. We therefore investigated whether TXNIP was dissociated from TRX and bound to NLRP3. A co-immunoprecipitation method was used to investigate the relationship between TXNIP, TRX, and NLRP3. After treatment with PPL for 1 h, we detected the dissociation of TRX from TXNIP (Fig. 4A). The dissociation occurred at low concentrations of PPL and was enhanced with increasing doses of PPL. At the same time, we detected ROS-dependent TXNIP-NLRP3 binding (Fig. 4B). This binding took place at low concentrations of PPL and was enhanced with increasing doses of PPL. Collectively, TXNIP was dissociated from TRX following the oxidation induced by PPL, and then TXNIP began binding to NLRP3.

3.6. Immunofluorescence staining analysis for the combination of NLRP3 and ASC or caspase-1

PPL induced the formation and activation of the NLRP3 inflammasome in RAW264.7 cells. We intended to validate the hypothesis that PPL induced the binding of ASC or caspase-1 to NLRP3 to activate the NLRP3 inflammasome. An immunofluorescence assay exhibited that the ASC protein was indeed expressed, and the expression and colocalization were augmented with increasing concentration (Fig. 5A). As shown in Fig. 5B, caspase-1 was expressed intracellularly, and its expression and colocalization with NLRP3 were also elevated with rising PPL dose. Confocal microscopic images showed PPL-induced colocalization of inflammasome molecules between NLRP3 (Red) and ASC

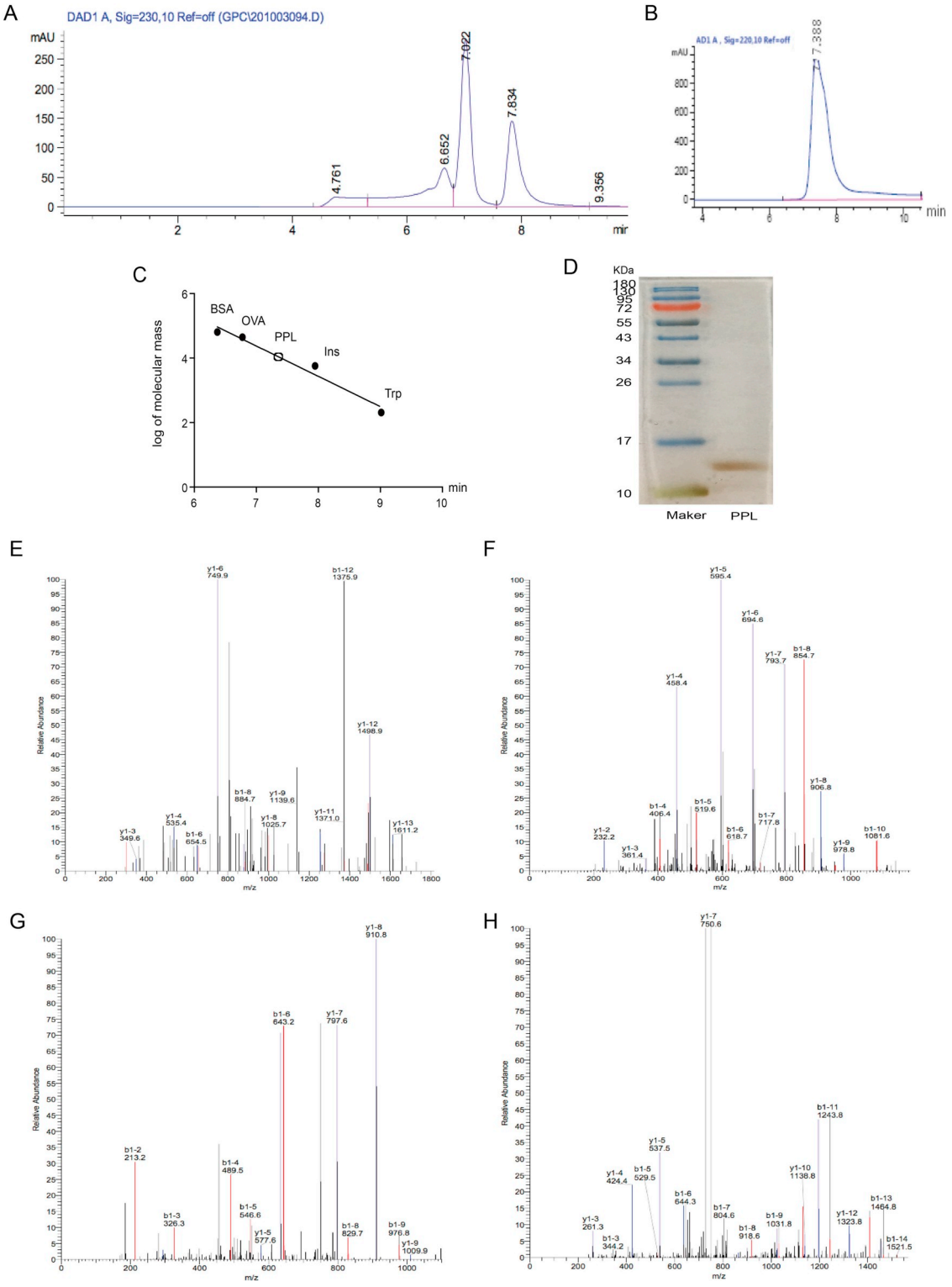

Fig. 1. Identification of PPL. (A) PPL was detected by size-exclusion high performance liquid chromatograph (SEC-HPLC). Tryptophan (0.2 kDa), insulin (5.7 kDa), ovalbumin (44 kDa), and bovine serum albumin (66.4 kDa) were used as standard markers. (B) PPL was detected by SEC-HPLC. (C) SEC-HPLC was used to plot the standard curve for native molecular weight of PPL. (D) SDS-PAGE showed a single band (about 13 kDa) of purified PPL. The gel was stained by silver nitrate. (E) MS/MS for peptide 'GELIIKDDDFQTIWSSR' from PPL. (F) MS/MS for peptide 'GNYALVVHPEGR' from PPL. (G) MS/MS for peptide 'LVIYGPSVFK' from PPL. (H) MS/MS for peptide 'LVMQGDCNLVLYGGK' from PPL.

(Green) or between NLRP3 (Red) and caspase-1 (Green), as evidenced by increased orange staining (or white spots in the "Mask" column in Fig. 5) in RAW264.7 cells. In order to investigate the relationship between ROS and NLRP3 inflammasome, PPL (50 μg/mL) was used to stimulate macrophages for 1 h after pretreatment with different doses of NAC for 0.5 h. As shown, such colocalization was blocked by NAC, which indicated a potential interaction between ROS and the NLRP3 inflammasome.

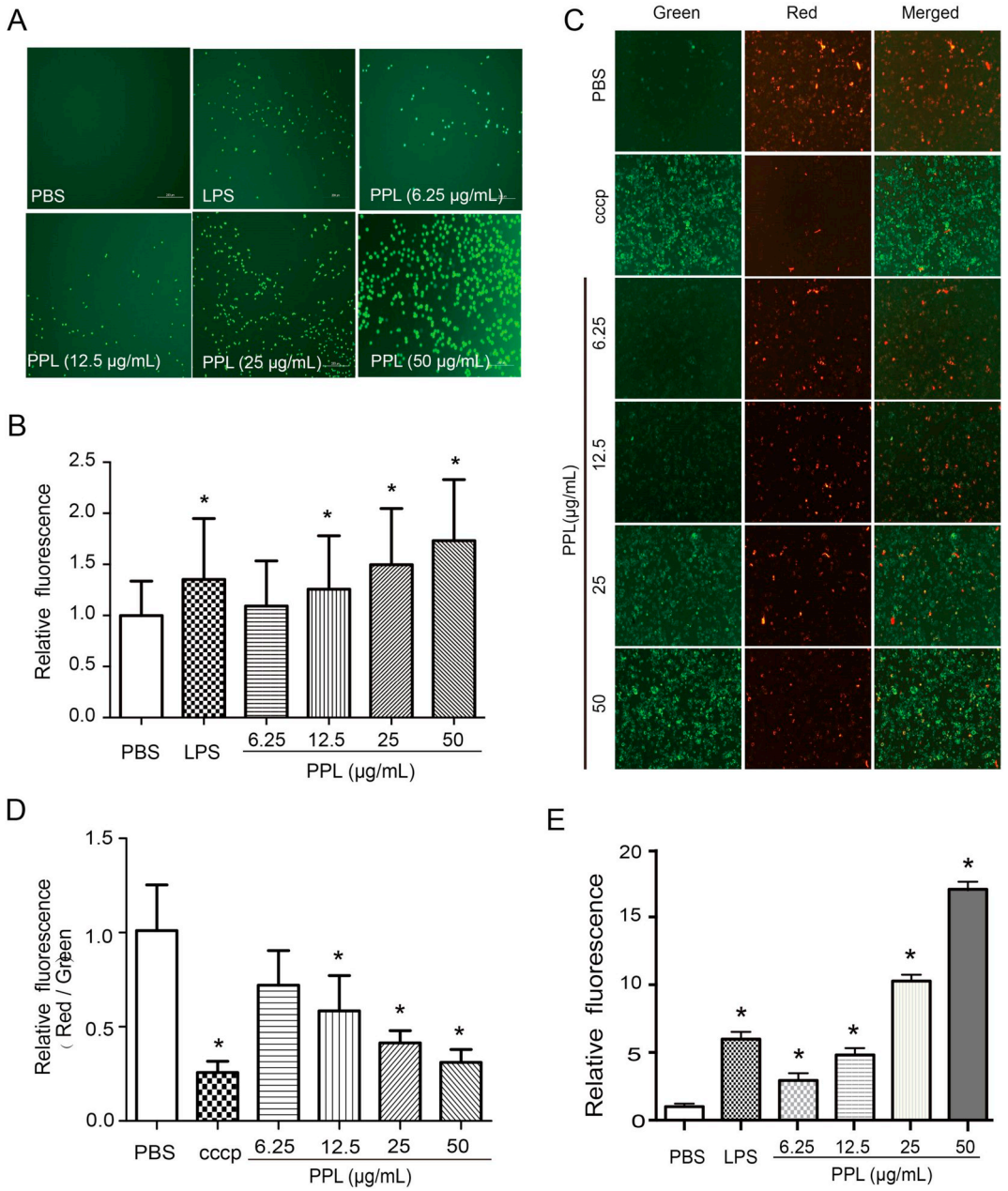

Fig. 2. Variations in ROS (A, B), MMP (C, D), and cytosolic free Ca^{2+} (E) induced in RAW264.7 cells treated for 1 h with PPL (6.25, 12.5, 25, or 50 μg/mL). Results are the mean ± SD ($n = 6$). *$P < 0.05$, compared with phosphate-buffered saline (PBS) (*t*-test). Images were acquired by microscopy, and the intensity was detected by a fluorescence microplate reader. CCCP, Carbonyl cyanide 3-chlorophenylhydrazone. LPS, Lipopolysaccharides.

3.7. The role of ROS in the inflammation caused by PPL

All NLRP3 activators are capable of inducing the production of ROS as common signals to activate the NLRP3 inflammasome, and both ROS inhibitors and scavengers can inhibit such activation [33]. PPL can stimulate macrophages to induce the massive production of ROS and IL-1β [4]. In order to investigate the mechanism of overproduction of IL-1β induced by ROS, PPL (50 μg/mL) was used to stimulate macrophages for 1 h after pretreatment with different doses of NAC for 0.5 h. In agreement with previous reports, addition of NAC reduced ROS (Fig. 6A). In particular, 12.5 mmol/L NAC led to a one-fold decrease. At the same time, NAC was able to inhibit the production of IL-1β and pro-IL-1β compared with the PPL group, and 12.5 mmol/L NAC led to a one-fold decrease (Fig. 6B, C). Simultaneously, after 12.5 mmol/L NAC pretreatment, the phosphorylation levels of p38, JNK, and ERK decreased two-fold, and p65 and IκB decreased four-fold (Fig. 6D, E). Therefore, NAC inhibited the MAPKs and NF-κB signaling pathways activated by PPL, further suppressing the production of pro-IL-1β and IL-1β. Also, the level of TXNIP was upregulated, unlike in the PPL group. The expression of caspase-1 p20 decreased dose-dependently (Fig. 6F), which further confirmed that the overproduction of ROS could activate NLRP3 inflammasome during the inflammation caused by PPL. According to the results above, ROS deficiency impaired activation of the MAPK and NF-κB pathways as well as the NLRP3 inflammasome and subsequent secretion of IL-1β.

3.8. PPL-induced pyroptosis in RAW264.7 cells

After treatment with different doses of PPL (6.25, 12.5, 25, or 50 μg/mL), the nuclei of RAW264.7 cells became pyknotic (the intensity of the blue fluorescence increased as the dose of PPL increased) and the plasma membrane became ruptured (the intensity of the red

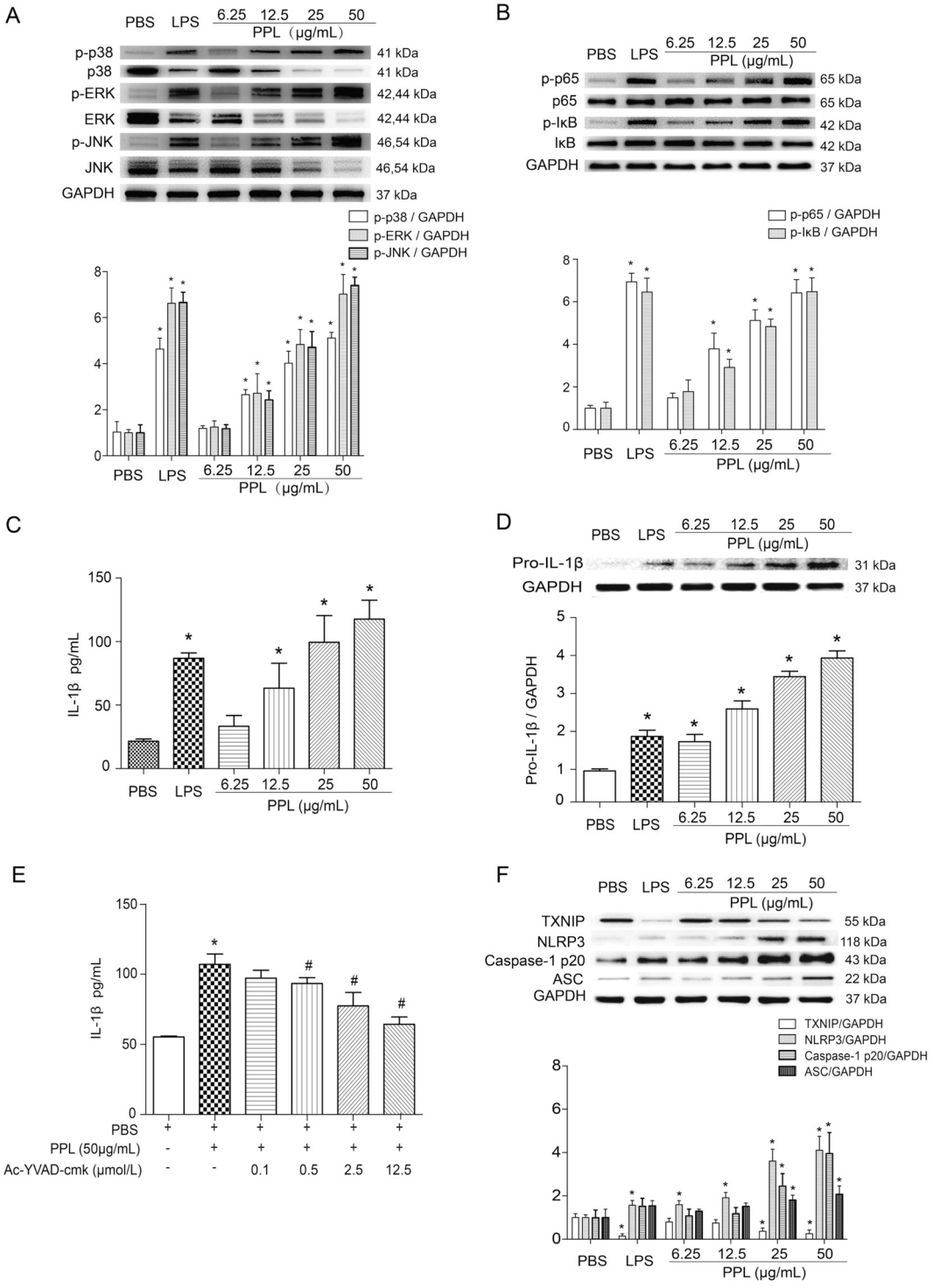

Fig. 3. The expression levels of (A) p-p38, p38, p-ERK, ERK, p-JNK, and JNK and (B) p-p65, p65, p-IκB, and IκB in RAW 264.7 cells treated for 1 h with PPL (6.25, 12.5, 25, or 50 μg/mL). (C) The release of IL-1β from RAW264.7 cells treated for 1 h with PPL (6.25, 12.5, 25, or 50 μg/mL). (D) The expression level of pro-IL-1β in RAW 264.7 cells treated for 1 h with PPL (6.25, 12.5, 25, or 50 μg/mL). (E) IL-1β released from macrophages stimulated by PPL (50 μg/mL) after pretreatment with different doses of Ac-YVAD-cmk, the caspase 1 inhibitor. (F) The expressions of NLRP3, caspase-1 p20, and ASC in RAW264.7 cells treated with PPL were upregulated, but TXNIP was downregulated. GAPDH served as the loading control. Results are expressed as mean ± SD (A, B, D, F, $n = 3$; C, E, $n = 6$) $^{*}P < 0.05$, compared with phosphate-buffered saline (PBS); $^{\#}P < 0.05$, compared with PPL (50 μg/mL) (*t*-test). IL, interleukin; Ac-YVAD-cmk, AC-TYR-VAL-ALA-ASP-CMK. LPS, Lipopolysaccharides.

fluorescence increased as the dose of PPL increased) (Fig. 7A). Over 3 h to 4 h, the proportion of cell pyroptosis greatly increased when RAW264.7 cells were exposed to PPL (50 μg/mL) (Fig. 7B). Moreover, different doses of NAC (0.1, 0.5, 2.5, and 12.5 mmol/L) inhibited cell pyroptosis after PPL treatment at 50 μg/mL (Fig. 7C), which demonstrated that ROS may be upstream of pyroptosis during PPL treatment. Considering the results shown in Sections 3.5 and 3.6, that is, activation of caspase-1 and the NLRP3 inflammasome with PPL treatment, we verified that the RAW264.7 cells underwent pyroptosis during the treatment of PPL. Pyroptosis is a proinflammatory form of

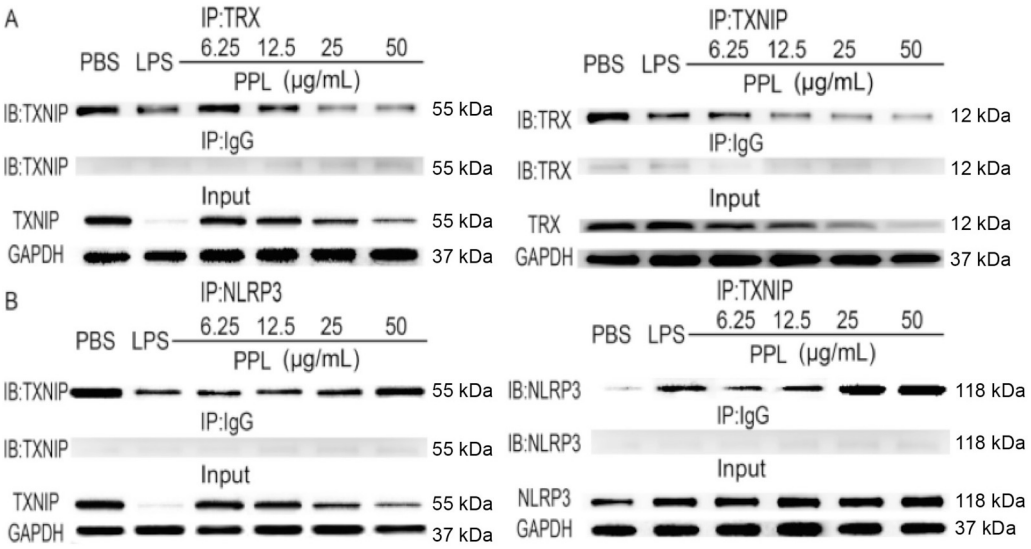

Fig. 4. PPL-induced dissociation of TXNIP from TRX, and binding of TXNIP with NLRP3. Interactions of TXNIP with TRX (A) or NLRP3 (B) were analyzed by immunoprecipitation and immunoblot assays. ROS induced the dissociation of TXNIP from TRX, allowing TXNIP to bind to NLRP3 ($n = 3$). LPS, Lipopolysaccharides.

death which depends on the enzymatic activation of inflammatory proteases that belong to the family of cysteine-dependent aspartate-specific proteases. The inflammasome-activated caspase-1 plays an important role in the induction of pyroptosis [34,35].

4. Discussion

P. pedatisecta, belonging to the Araceae family, has been widely used in the Chinese herbal market for its great efficacy in stopping vomiting, relieving cough, reducing sputum, and relieving pain [1]. Several

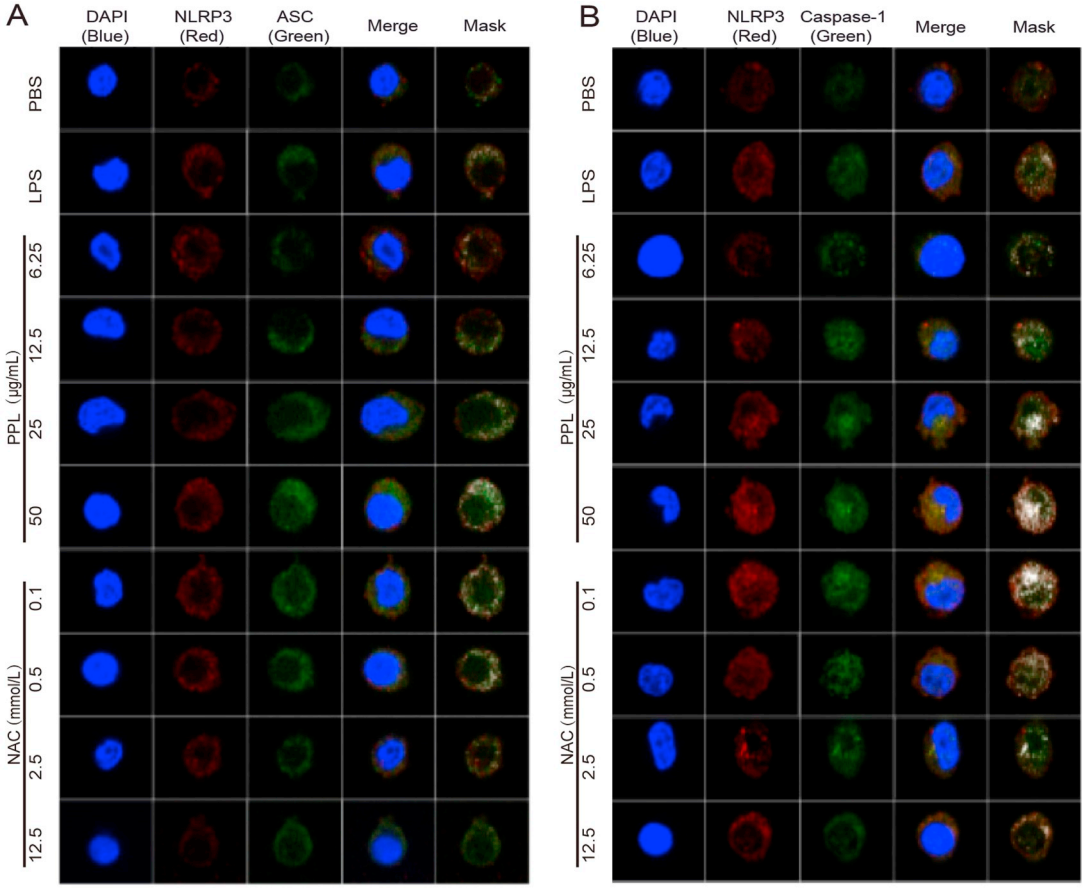

Fig. 5. Colocalization of NLRP3 inflammasome components. Representative confocal fluorescence images show the colocalization of NLRP3 with ASC (A) or caspase-1 (B). PPL-induced colocalization of inflammasome molecules between NLRP3 (red) and ASC (green) or between NLRP3 (red) and caspase-1 (green), as shown by increased white staining (white spots) in RAW264.7 cells. Such colocalization was blocked by the ROS inhibitor (NAC) ($n = 6$). NAC, *N*-acetylcysteine. LPS, Lipopolysaccharides. (For interpretation of the references to color in this figure legend, the reader is referred to the web version of this article.)

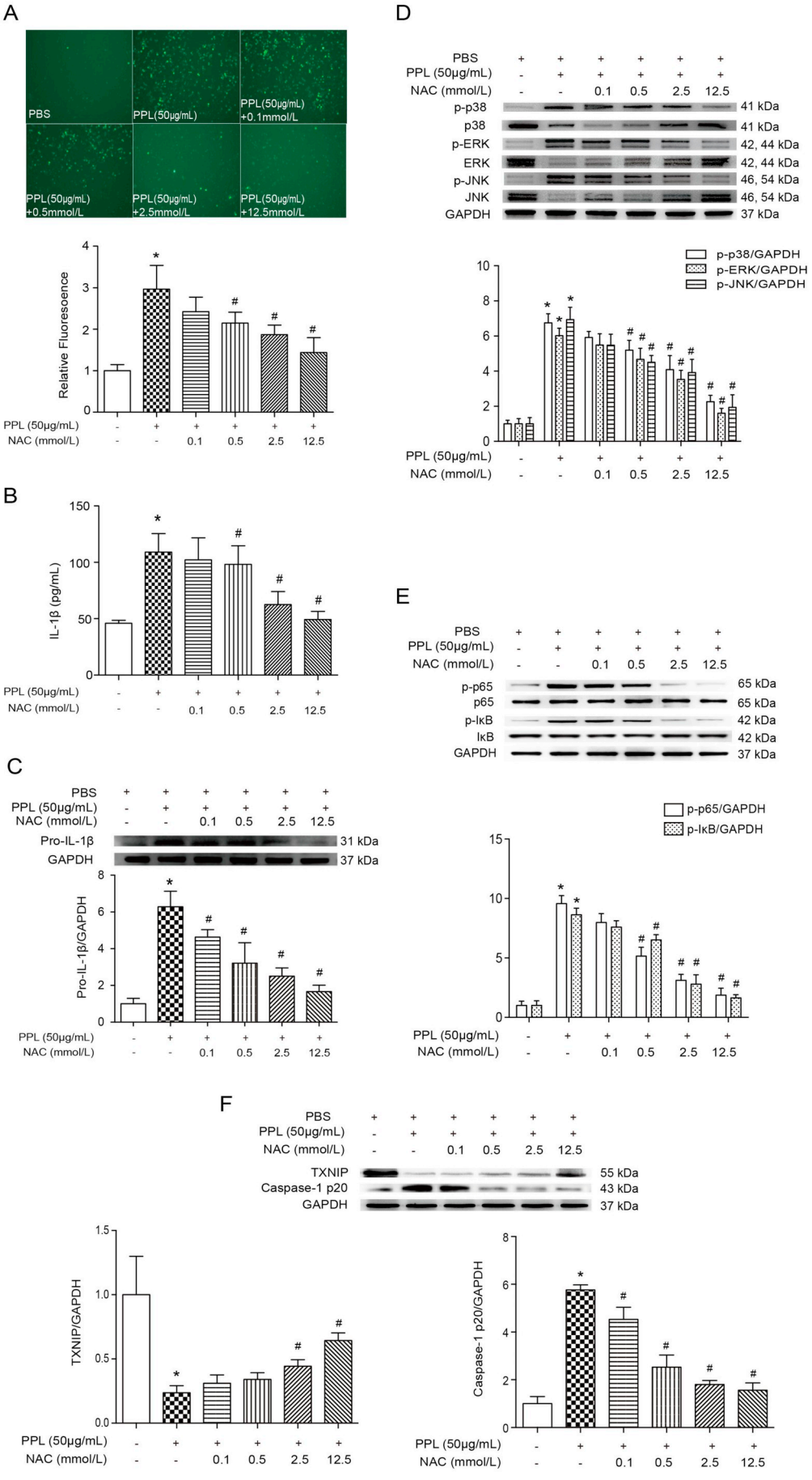

Fig. 6. Release of IL-1β and the expressions of the MAPK, NF-κB, and NLRP3 signaling pathways after NAC treatment. (A) Differences between the level of ROS stimulated by PPL (50 μg/mL) after pretreatment with different concentrations of NAC. (B) Level of IL-1β released from macrophages stimulated by PPL (50 μg/mL) after pretreatment with NAC. (C) Western blot of pro-IL-1β in RAW264.7 cells stimulated by PPL after NAC treatment. Compared with the 50 μg/mL PPL-stimulated group, NAC dose-dependently downregulated the levels of pro-IL-1β. (D) Western blot of MAPKs in RAW264.7 cells stimulated by PPL after NAC treatment. Compared with the 50 μg/mL PPL-stimulated group, NAC dose-dependently downregulated the levels of p-p38, p-JNK, and p-ERK. (E) NAC reduced the levels of p-p65 and p-IκB dose-dependently. (F) NAC dose-dependently increased the level of TXNIP and reduced the level of caspase-1 p20. Results are expressed as mean ± SD (A, B, $n = 6$; C, D, E, F, $n = 3$). $^{*}P < 0.05$, compared with phosphate-buffered saline (PBS); $^{\#}P < 0.05$, compared with PPL (50 μg/mL). IL, interleukin; NAC, *N*-acetylcysteine.

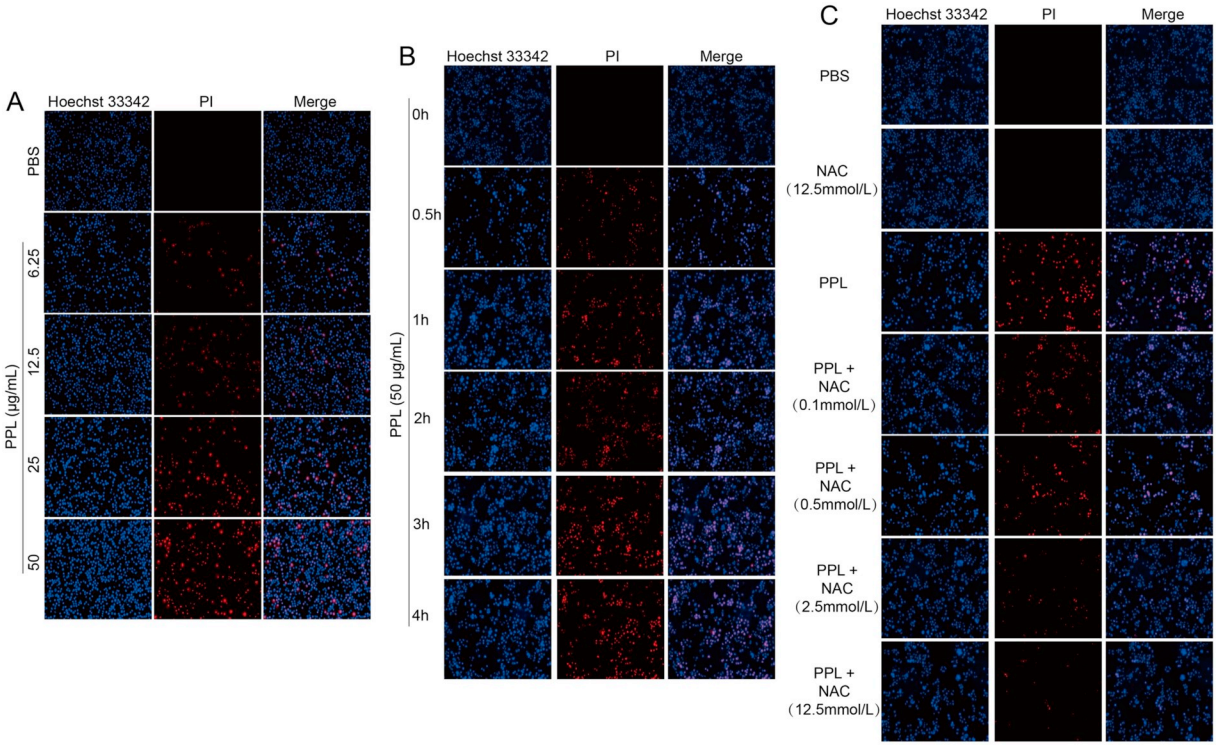

Fig. 7. PPL-induced pyroptosis in RAW264.7 cells. (A) The nuclei of RAW264.7 cells became pyknotic (the intensity of the blue fluorescence increased as the dose of PPL increased) and the plasma membrane ruptured (the intensity of the red fluorescence increased as the dose of PPL increased). (B) PPL (50 μg/mL)-induced pyroptosis in RAW264.7 cells. Over time (0.5, 1, 2, 3, and 4 h), the proportion of cell pyroptosis increased. (C) Different doses of NAC (0.1, 0.5, 2.5, and 12.5 mmol/L) inhibited cell pyroptosis under PPL treatment (50 μg/mL). PI, Propidium iodide. NAC, *N*-acetylcysteine. (For interpretation of the references to color in this figure legend, the reader is referred to the web version of this article.)

prescriptions containing *P. pedatisecta*, such as 'GongJingAiShuan,' have been employed in the treatment of cervical cancer and cervical precancerous lesions. Although *P. pedatisecta* has great effects in treating certain diseases, we still cannot ignore its toxicity, which has been a major bottleneck in its development as a drug.

Our previous study has demonstrated that the toxicity of *P. pedatisecta* was closely related to PPL [4]. Lectin, a kind of protein mainly existing in plants and animals, occupies a leading position in cell adhesion. Some lectins cause inflammation and even cell death [36–38]. PPL has been proven to have significant proinflammatory ability and can induce the release of inflammatory factors [39]. *In vitro* studies have demonstrated that PPL can induce macrophages to produce excessive amounts of ROS and IL-1β [4], but the specific mechanism is still unknown.

Herein, we explored the underlying mechanism of the inflammation induced by PPL. As we all know, ROS play important roles in the signal transduction of inflammation [5]. After stimulation of cells by an irritant, ROS may increase, which can be followed by a decrease in MMP and an increase in cytosolic free Ca^{2+} concentration [8–10]. In our study, PPL caused the overproduction of ROS, together with a drop in MMP and the release of cytosolic free Ca^{2+}. Then, the levels of p-p38, p-JNK, p-ERK, p-p65, p-IκB, pro-IL-1β, and IL-1β were dose-dependently increased by PPL, indicating that the MAPK and NF-κB signaling pathways were activated and that PPL did exert a proinflammatory activity. In our research, there was a decrease in the total proteins of p38, ERK and JNK under the treatment of PPL, we hypothesized the reason was associated with its inhibition of the mRNA expressions of p38, ERK and JNK (Supplementary Fig. 1) or activation of certain inhibitory proteins. The specific mechanism remains to be further studied. Also, the production of p-p38, p-JNK, p-ERK, p-p65, p-IκB, pro-IL-1β, and IL-1β were reduced by NAC. Therefore, during the inflammation caused by PPL, ROS were likely upstream of the MAPK and NF-κB signaling pathways.

The level of IL-1β was decreased by adding a caspase-1 inhibitor (Ac-YVAD-cmk), which indicated that the PPL-induced release of IL-1β was closely related to caspase-1 and the NLRP3 inflammasome, since caspase-1 is one of the components of the NLRP3 inflammasome [40]. According to our research, under PPL stimulation, the NLRP3 inflammasome was activated with TXNIP bound to NLRP3. There was colocalization of NLRP3 with ASC and caspase-1, which then promoted the activation of caspase-1 and caused pro-IL-1β to become IL-1β. Furthermore, the activation of the NLRP3 inflammasome was inhibited by NAC, which indicated that ROS may be upstream of the NLRP3 inflammasome.

The results shown above revealed that PPL promoted the maturation and secretion of IL-1β by activating the ROS, MAPK, NF-κB, and TXNIP-NLRP3-IL-1β signaling pathways, further leading to inflammatory cascades and intense inflammatory stimuli (Fig. 8). ROS may be key molecular targets involved in the proinflammatory response cause by PPL. The MAPKs, NF-κB, and NLRP3 signaling pathways included upstream signaling molecules for the release of IL-1β under PPL stimulation.

PPL was associated with pyroptosis of RAW264.7 cells, showing nuclei being pyknotic and plasma membranes being ruptured. Pyroptosis [41,42], a pattern of programmed cell death, is caused by activation of a caspase-specific protease after the inflammasome senses a pathogen signal. Pyroptosis is characterized by both necrosis and apoptosis in morphology. Similar to apoptosis, pyroptosis cells featured nuclear shrinkage and chromatin DNA breaking. Unlike apoptosis, many pores of 1–2 nm are formed on the membranes of pyroptotic cells, which leads to the loss of integrity of the cell membranes [43]. The loss results in the membrane being unable to regulate the entry and exit of substances, eventually causing it to dissolve and the content of the cells to be released, which results in the induction of the inflammatory

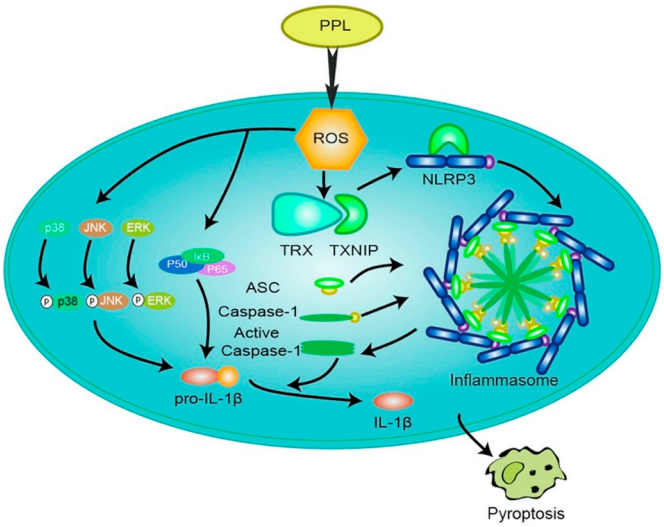

Fig. 8. Signaling pathways involved in inflammation induced by PPL. After PPL stimulated macrophages, MMP decreased and oxidative stress occurred, releasing a large amount of ROS. ROS activated both MAPKs and NF-κB signaling pathways to promote the production of pro-IL-1β. Activation of NLRP3 signaling activated caspase-1, resulting in the maturation of IL-1β and subsequently cell pyroptosis.

response [41]. At the same time, the cells release IL-1β and IL-18 to recruit more inflammatory cells to expand the inflammatory response [34].

Recent studies have demonstrated that ROS may be an upstream mechanism implicated in cell pyroptosis [44,45]. In agreement with this view, our study showed that cell pyroptosis induced by PPL could be inhibited by NAC, an ROS scavenger. This revealed a close relationship between ROS and pyroptosis, and that ROS may be upstream of cell pyroptosis. Combined with the results mentioned above, that is, the observation that PPL could induce the activation of the NLRP3 inflammasome and promote caspase-1 to active caspase-1 p20, it was further confirmed that PPL was associated with the pyroptosis of RAW264.7 cells.

Collectively, for the first time, we herein linked the proinflammatory activity of PPL with oxidative stress that led to an overproduction of ROS; activation of the MAPK, NF-κB, and NLRP3 signaling transduction pathways; and the release of inflammatory factor IL-1β, which then led to pyroptosis of RAW264.7 cells. Therefore, based on our current research results, PPL is expected to be used as a possible drug in studies related to the induction of the oxidative stress response. The findings suggest a new natural plant-derived proinflammatory agent as a basis for future studies on anti-inflammatory drugs and on the processing of *P. pedatisecta*, a widely used herb in Chinese medicine for relieving cough and reducing sputum. Furthermore, this study provides a reference for improving and innovating processing methods of toxic Chinese medicines from the Araceae family, and for the clinical use of toxic Chinese medicines.

Supplementary data to this article can be found online at https://doi.org/10.1016/j.intimp.2018.11.002.

Author contributions

Hongli Yu and Hao Wu designed and directed the research; Wei Wang, Shanhu Mao, Hongli Yu, Xuelian Shan, Xingde Zhang, Guojing Cui, Xianqiong Liu are responsible for research and data analysis tasks; this article was written by Wei Wang under the direction of Hongli Yu.

Acknowledgments

This research is sponsored by the National Natural Science Foundation of China (No. 81573605) and a project funded by the Postgraduate Research & Practice Innovation Program of Jiangsu Province (KYCX18_1609). In addition, thanks to my school, Nanjing University of Chinese Medicine. We thank LetPub (www.letpub.com) for its linguistic assistance during the preparation of this manuscript.

Conflicts of interest

The authors declare no conflict of interest.

References

[1] Li Wei, Handbook of Chinese Herbal Medicine Identification in South China [M], People's Military Medical Press, Beijing, 2012.
[2] Xianqiong Liu. A study on correlation between lectin from Araceae and toxity (Article in Chinese). 2012.
[3] Yaozong Pan. Study on the toxicity mechanism of Araceae (Article in Chinese). 2016.
[4] S.H. Mao, H.L. Yu, H. Wu, W. Wang, X.N. Li, Pro-inflammatory mechanism of lectin from *Pinellia pedatisecta* on macrophage, Zhongguo Zhong Yao Za Zhi. 42 (2017) 2497–2502.
[5] T.A. Tabish, S. Zhang, P.G. Winyard, Developing the next generation of graphene-based platforms for cancer therapeutics: the potential role of reactive oxygen species, Redox Biol. 22 (2017) 34–40 https://doi.org/10.1016/j.redox.2017.11.018.
[6] X.F. Liu, F. Ye, H.B. Xiong, D.N. Hu, A. Limb, T. Xie, L. Peng, W. Yang, Y.B. Sun, M.M. Zhou, E. Song, D.Y. Zhang, IL-1β Upregulates IL-8 production in human Müller cells through activation of the p38 MAPK and ERK1/2 signaling pathways, Inflammation 37 (2014) 1486–1495 https://doi.org/10.1007/s10753-014-9874-5.
[7] Q. He, H. You, X.M. Li, T.H. Liu, P. Wang, B.E. Wang, HMGB1 promotes the synthesis of pro-IL-1β and pro-IL-18 by activation of p38 MAPK and NF-κB through receptors for advanced glycation end-products in macrophages, Asian Pac. J. Cancer Prev. 13 (2012) 1365–1370.
[8] N. Tajeddine, How do reactive oxygen species and calcium trigger mitochondrial membrane permeabilisation, Biochim. Biophys. Acta 1860 (2016) 1079–1088, https://doi.org/10.1016/j.bbagen.2016.02.013.
[9] D. Thummuri, M.K. Jeengar, S. Shrivastava, A. Areti, V.G. Yerra, S. Y, P. K, N.V. M, A. Kumar, R. Sistla, Boswellia ovalifoliolata, abrogates ROS mediated NF-κB activation, causes apoptosis and chemosensitization in triple negative breast cancer cells, Environ. Toxicol. Pharmacol. 38 (2014) 58–70 https://doi.org/10.1016/j.etap.2014.05.002.
[10] K.Y. Kim, H.J. Cho, S.N. Yu, S.H. Kim, H.S. Yu, Y.M. Park, N. Mirkheshti, S.Y. Kim, C.S. Song, B. Chatterjee, S.C. Ahn, Interplay of reactive oxygen species, intracellular Ca2+ and mitochondrial homeostasis in the apoptosis of prostate cancer cells by deoxypodophyllotoxin, J. Cell. Biochem. 114 (2013) 1124–1134 https://doi.org/10.1002/jcb.24455.
[11] J.E. Lee, M.S. Lim, J.H. Park, C.H. Park, H.C. Koh, Nuclear NF-κB contributes to chlorpyrifos-induced apoptosis through p53 signaling in human neural precursor cells, Neurotoxicology 42 (2014) 58–70 https://doi.org/10.1016/j.neuro.2014.04.001.
[12] X. Meng, S.M.A.P.K. Zhang, Cascades in plant disease resistance signaling, Annu. Rev. Phytopathol. 51 (2013) 245–266 https://doi.org/10.1146/annurev-phyto-082712-102314.
[13] J.H. Song, K.S. Kang, Y.K. Choi, Protective effect of casuarinin against glutamate-induced apoptosis in HT22 cells through inhibition of oxidative stress-mediated MAPK phosphorylation, Bioorg. Med. Chem. Lett. 27 (2017) 5109–5113 https://doi.org/10.1016/j.bmcl.2017.10.075.
[14] A. Dolunay, S.P. Senol, M. Temiz-Resitoglu, D.S. Guden, A.N. Sari, S. Sahan-Firat, B. Tunctan, Inhibition of NLRP3 Inflammasome prevents LPS-induced inflammatory hyperalgesia in mice: contribution of NF-κB, caspase-1/11, ASC, NOX, and NOS isoforms, Inflammation 40 (2017) 366–386 https://doi.org/10.1007/s10753-016-0483-3.
[15] S.T. Yao, F. Cao, J.L. Chen, NLRP3 is required for complement-mediated caspase-1 and IL-1β activation in ICH, Short Title for Running Head: NLRP3 is Required for ICH, J. Mol. Neurosci. 61 (2017) 385–395 https://doi.org/10.1007/s12031-016-0874-9.
[16] C.C. Lin, B.T. Edelson, New insights into the role of IL-1β in experimental autoimmune encephalomyelitis and multiple sclerosis, J. Immunol. 198 (2017) 4553–4560 https://doi.org/10.4049/jimmunol.1700263.
[17] M.H. Lv, H.Z. Zeng, Y. He, J.S. Zhang, G. Tan, Dexmedetomidine promotes liver regeneration in mice after 70% partial hepatectomy by suppressing NLRP3 inflammasome not TLR4/NF-κB, Int. Immunopharmacol. 54 (2018) 46–51 https://doi.org/10.1016/j.intimp.2017.10.030.
[18] R. Zhou, A.S. Yazdi, P. Menu, J. Tschopp, A role for mitochondria in NLRP3 inflammasome activation, Nature 469 (2011) 221–225 https://doi.org/10.1038/nature09663.
[19] X. Deng, W. Huang, J. Peng, T.T. Zhu, X.L. Sun, X.Y. Zhou, H. Yang, J.F. Xiong, H.Q. He, Y.H. Xu, Y.Z. He, Irisin alleviates advanced glycation end products-induced inflammation and endothelial dysfunction via inhibiting ROS-NLRP3

inflammasome signaling, Inflammation 41 (2018) 260–275 https://doi.org/10.1007/s10753-017-0685-3.
[20] Y. Hou, Y. Wang, Q. He, L. Li, H. Xie, Y. Zhao, J. Zhao, Nrf2 inhibits NLRP3 inflammasome activation through regulating Trx1/TXNIP complex in cerebral ischemia reperfusion injury, Behav. Brain Res. 336 (2018) 32–39 https://doi.org/10.1016/j.bbr.2017.06.027.
[21] Y. Song, R. Sun, Z. Ji, X. Li, Q. Fu, S. Ma, Perilla aldehyde attenuates CUMS-induced depressive-like behaviors via regulating TXNIP/TRX/NLRP3 pathway in rats, Life Sci. 206 (2018) 117–124 https://doi.org/10.1016/j.lfs.2018.05.038.
[22] Z. Rao, F. Xu, T. Wen, F. Wang, W. Sang, N. Zeng, Protective effects of essential oils from Rimulus cinnamon on endotoxin poisoning mice, Biomed. Pharmacother. 101 (2018) 304–310 http://10.1016/j.biopha.2018.02.092.
[23] S.A. Conos, K.E. Lawlor, D.L. Vaux, J.E. Vince, L.M. Lindqvist, Cell death is not essential for caspase-1-mediated interleukin-1β activation and secretion, Cell Death Differ. 23 (2016) 1827–1838 http://10.1038/cdd.2016.69.
[24] H.L. Yu, T.F. Zhao, H. Wu, Y.Z. Pan, Q. Zhang, K.L. Wang, C.C. Zhang, Y.P. Jin, Pinellia ternata lectin exerts a pro-inflammatory effect on macrophages by inducing the release of pro-inflammatory cytokines, the activation of the nuclear factor-κB signaling pathway and the overproduction of reactive oxygen species, Int. J. Mol. Med. 36 (2015) 1127–1135 https://doi.org/10.3892/ijmm.2015.2315.
[25] P.R. Pereira, E.M. Del Aguila, M.A. Verícimo, R.B. Zingali, V.M. Flosi Paschoalin, Silva J.T. Purification, Characterization of the lectin from Taro (*Colocasia esculenta*) and its effect on mouse splenocyte proliferation in vitro and in vivo, Protein J. 33 (2014) 92–99 https://doi.org/10.1007/s10930-013-9541-y.
[26] E.K. Kim, E.J. Choi, Compromised MAPK signaling in human diseases: an update, Arch. Toxicol. 89 (2015) 867–882 http://10.1007/s00204-015-1472-2.
[27] J.M. Kyriakis, J. Avruch, Mammalian MAPK signal transduction pathways activated by stress and inflammation: a 10-year update, Physiol. Rev. 92 (2012) 689–737 http://10.1152/physrev.00028.2011.
[28] S. Ruey-Horng, C.Y. Wang, C.M. Yang, NF-kappaB signaling pathways in neurological inflammation: a mini review, Front. Mol. Neurosci. 8 (2015) 77 http://10.3389/fnmol.2015.00077.
[29] T. Chiba, H. Inoko, M. Kimura, T. Sato, Role of nuclear IκBs in inflammation regulation, Biomol. Concepts 4 (2013) 187–196 http://10.1515/bmc-2012-0039.
[30] G. Chen, M.H. Shaw, Y.G. Kim, G. Nunez, Nod-like receptors: role in innate immunity and inflammatory disease, Annu. Rev. Pathol. 4 (2009) 365–398, https://doi.org/10.1146/annurev.pathol.4.110807.092239.
[31] E. Yoshihara, S. Masaki, Y. Matsuo, Z. Chen, H. Tian, J. Yodoi, Thioredoxin/Txnip: redoxisome, as a redox switch for the pathogenesis of diseases, Front. Immunol. 4 (2013) 514 http://10.3389/fimmu.2013.00514.
[32] R. Zhou, A. Tardivel, B. Thorens, I. Choi, J. Tschopp, Thioredoxin-interacting protein links oxidative stress to inflammasome activation, Nat. Immunol. 11 (2010) 136–140 https://doi.org/10.1038/ni.1831.
[33] C. Dostert, V. Petrilli, R. van Bruggen, C. Steele, B.T. Mossman, J. Tschopp, Innate immune activation through Nalp3 inflammasome sensing of asbestos and silica, Science 320 (2008) 674–677 https://doi.org/10.1126/science.1156995.
[34] I. Jorgensen, E.A. Miao, Pyroptotic cell death defends against intracellular pathogens, Immunol. Rev. 265 (2015) 130–142 http://10.1111/imr.12287.
[35] G. Sollberger, G.E. Strittmatter, M. Garstkiewicz, J. Sand, H.D. Beer, Caspase-1: the inflammasome and beyond, Innate Immun. 20 (2014) 115–125 http://10.1177/1753425913484374.
[36] I. Hasan, S. Sugawara, Y. Fujii, Y. Koide, D. Terada, N. Iimura, T. Fujiwara, K.G. Takahashi, N. Kojima, S. Rajia, S.M. Kawsar, R.A. Kanaly, H. Uchiyama, M. Hosono, Y. Ogawa, H. Fujita, J. Hamako, T. Matsui, Y. Ozeki, MytiLec, a mussel R-type lectin, interacts with surface glycan Gb3 on Burkitt's lymphoma cells to trigger apoptosis through multiple pathways, Mar. Drugs 13 (2015) 7377–7389 https://doi.org/10.3390/md13127071.
[37] X.Q. Liu, H. Wu, H.L. Yu, T.F. Zhao, Y.Z. Pan, R.J. Shi, Purification of a lectin from *Arisaema erubescens* (Wall.) Schott and its pro-inflammatory effects, Molecules 16 (2011) 9480–9494 https://doi.org/10.3390/molecules16119480.
[38] M.C. Silva, C.A. de Paula, J.G. Ferreira, E.J. Paredes-Gamero, A. Vaz, M.U. Sampaio, M.T. Correia, M.L. Oliva, Bauhinia forficata lectin (BfL) induces cell death and inhibits integrin-mediated adhesion on MCF7 human breast cancer cells, Biochim. Biophys. Acta 1840 (2014) 2262–2271, https://doi.org/10.1016/j.bbagen.2014.03.009.
[39] H.L. Yu, Q. Zhang, H. Wu, C. Shao, T.F. Zhao, Z. Li, Comparative study on pro-inflammatory toxicity of Pinellia pedatiecta before and after being processed with alum, Zhongguo Zhong Yao Za Zhi. 38 (2013) 3893–3897.
[40] S. Koka, M. Xia, Y. Chen, O.M. Bhat, X.X. Yuan, K.M. Boini, P.S. Li, Endothelial NLRP3 inflammasome activation and arterial neointima formation associated with acid sphingomyelinase during hypercholesterolemia, Redox Biol. 13 (2017) 336–344 https://doi.org/10.1016/j.redox.2017.06.004.
[41] T. Bergsbaken, S.L. Fink, B.T. Cookson, Pyroptosis: host cell death and inflammation, Nat. Rev. Microbiol. 7 (2009) 99–109 https://doi.org/10.1038/nrmicro2070.
[42] T. Dong, D. Liao, X. Liu, X. Lei, Using small molecules to dissect non-apoptotic programmed cell death: necroptosis, ferroptosis, and pyroptosis, Chembiochem 16 (2016) 2557–2561 http://10.1002/cbic.201500422.
[43] S.L. Fink, B.T. Cookson, Caspase-1-dependent pore formation during pyroptosis leads to osmotic lysis of infected host macrophages, Cell. Microbiol. 8 (2006) 1812–1825 http://10.1111/j.1462-5822.2006.00751.x.
[44] Yoonjeong Jang, Ah. Young Lee, Sang-Hee Jeong, Kyung-Hun Park, Min-Kyoung Paik, Nam-Joon Cho, Ji-Eun Kim, Myung-Haing Cho, Chlorpyrifos induces NLRP3 inflammasome and pyroptosis/apoptosis via mitochondrial oxidative stress in human keratinocyte HaCaT cells, Toxicology 338 (2015) 37–46 http://10.1016/j.tox.2015.09.006.
[45] X. Zhang, J. Luan, W. Chen, J. Fan, Y. Nan, Y. Wang, Y. Liang, G. Meng, D. Ju, Mesoporous silica nanoparticles induced hepatotoxicity via NLRP3 inflammasome activation and caspase-1-dependent pyroptosis, Nanoscale (2018), https://doi.org/10.1039/c8nr00554k.